

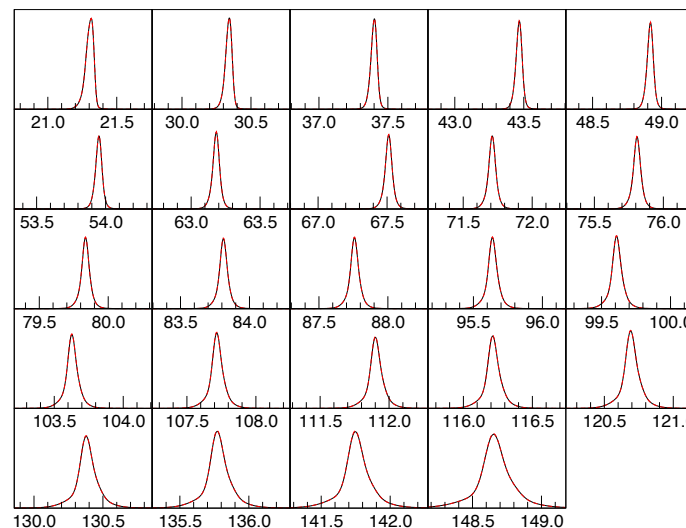
Computing Powder Diffraction Line Shapes with the Fundamental Parameters Approach

Marcus H. Mendenhall,
NIST, Gaithersburg, Maryland, USA

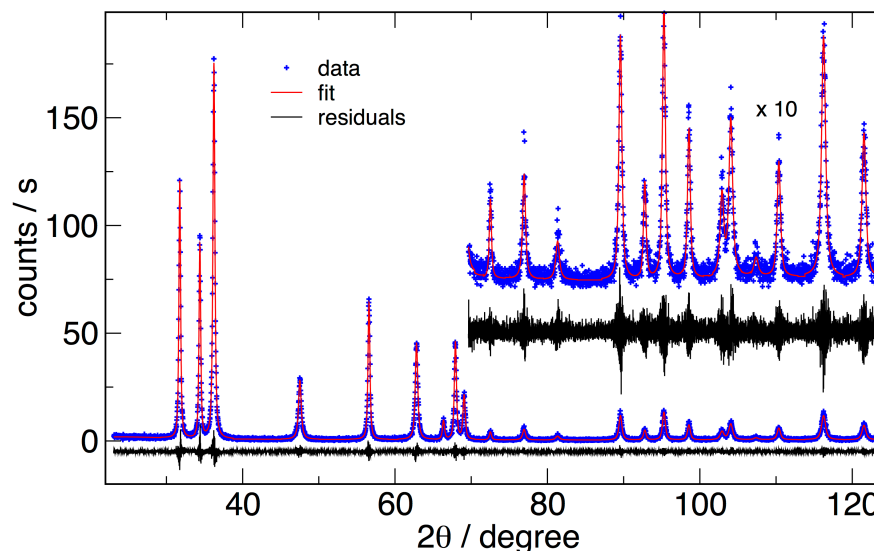
collaborator: James Cline

What is the problem?

- SRM 660b peak shapes. 660b is LaB_6 , intrinsic peaks are extremely sharp due to large, unstrained crystallites. These are for the NIST DBD with an IBM. They are not sharp, and their shape shifts with angle.



- SRM 1979 '15 nm' peak shapes. Peaks are very broadened by microstructure. Aberrations, as determined from, for example, SRM 660x, must be accounted for to get microstructure. These are measured on the NIST DBD with an IBM.



Why compute shapes?

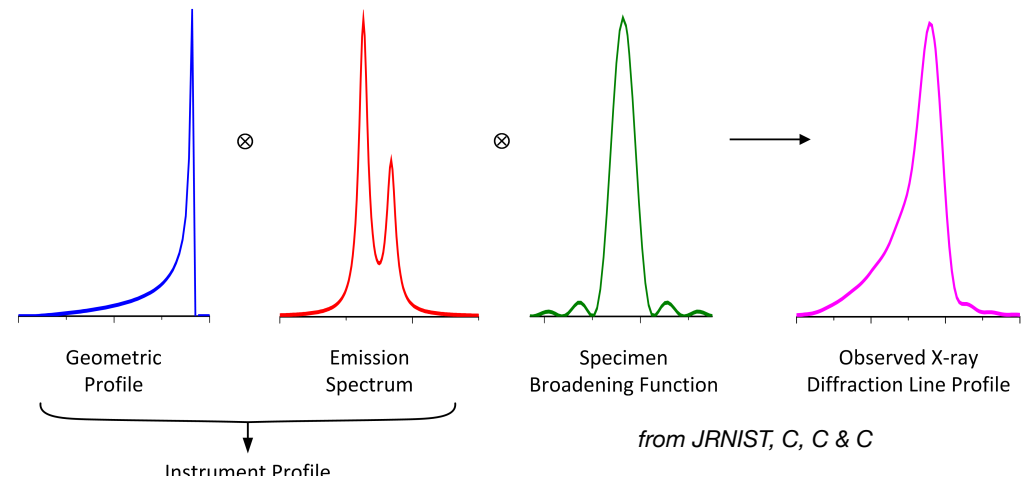
- Analysis of powder diffraction patterns is carried out for numerous reasons:
 - determination of lattice parameters
 - determination of crystal structure
 - determination of mixed material composition
- All of these are most accurately done with either Rietveld or Pawley fitting of a complete pattern, which reduces the number of free parameters and can be robust against noise
- Such fits require accurate peak models. Ad hoc parameterized models are commonly used, and work pretty well for structure and composition. They do not work too well for lattice measurement.

Important references

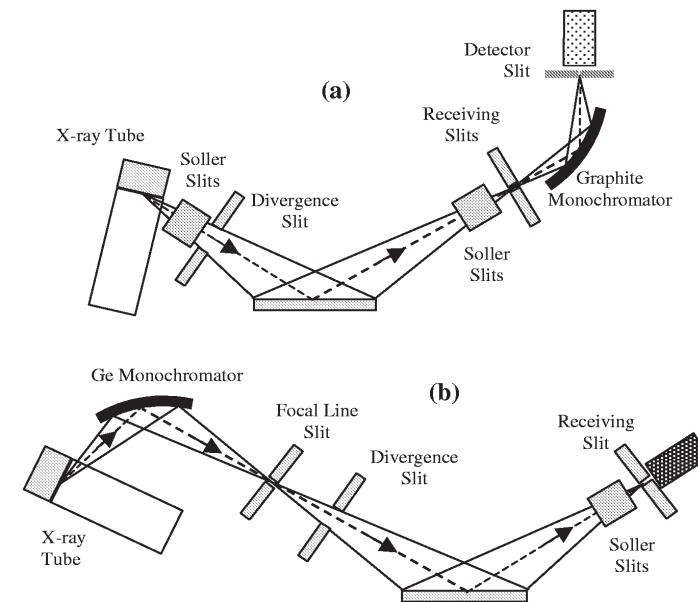
- Wilson, A. J. C, X-ray optics, 2nd ed., Methuen Press, London, 1962
- Cheary, R. W. & Coelho, A. A.
Axial Divergence in a Conventional X-ray Powder Diffractometer. I. Theoretical Foundations
Journal of Applied Crystallography, International Union of Crystallography, **1998**, 31, 851-861
- Cheary, R. W. & Coelho, A. A.
Axial Divergence in a Conventional X-ray Powder Diffractometer. II. Realization and Evaluation in a Fundamental-Parameter Profile Fitting Procedure
Journal of Applied Crystallography, International Union of Crystallography, **1998**, 31, 862-868
- Cheary, R. W.; Coelho, A. A. & Cline, J. P.
Fundamental Parameters Line Profile Fitting in Laboratory Diffractometers
J. Res. NIST, **2004**, 109, 1-25 (*note: we refer to this as C, C & C in credits*)
- Cline, Mendenhall, Black, Windover, & Henins
The Optics and Alignment of the Divergent Beam Laboratory X-ray Powder Diffractometer and its Calibration Using NIST Standard Reference Materials, *J. Res. NIST*, **2015**, 120
<http://dx.doi.org/10.6028/jres.120.013> (*note: VolH in credits*)
- Marcus H. Mendenhall, Katharine Mullen, and James P. Cline
An Implementation of the Fundamental Parameters Approach for Analysis of X-ray Powder Diffraction Line Profiles, *J. Res. NIST*, **2015**, 120 (*note: FPAPC in credits*)
Sample code available at: <http://dx.doi.org/10.6028/jres.120.014.c>

What creates observed line shape?

- In a simple theory, a line profile is a convolution of effects from various uncorrelated sources.



- WARNING:** only true if sources do not have correlated contributions. This is not strictly true, and full Monte Carlo ray tracing is useful to compare to convolution assumption.



from JRNIST, C, C & C, fig. 3

The convolution theorem

- ‘smearing’ of two functions together is convolution

$$[f \otimes g](t) = \int_{-\infty}^{+\infty} f(\tau) g(t - \tau) d\tau$$

- for discretely sampled functions of length n computation time is n^2

$$\mathcal{F}(f(t))(\omega) = \int_{-\infty}^{+\infty} f(t) e^{-i\omega t} dt$$

- this is expensive for large values

$$\mathcal{F}([f \otimes g](t))(\omega) = \mathcal{F}(f(t))(\omega) \times \mathcal{F}(g(t))(\omega)$$

or, in short,

- Fourier convolutions need time $n \log(n)$: much faster

$$\mathcal{F}(f \otimes g \otimes h \dots) = \mathcal{F}(f) \times \mathcal{F}(g) \times \mathcal{F}(h) \dots$$

- Beware periodicity!

Fourier transform properties

Translation / time shifting

For any real number x_0 , if $h(x) = f(x - x_0)$, then $\hat{h}(\xi) = e^{-2\pi i x_0 \xi} \hat{f}(\xi)$.

https://en.wikipedia.org/wiki/Fourier_transform

Modulation / frequency shifting

For any real number ξ_0 if $h(x) = e^{-2\pi i x \xi_0} f(x)$, then $\hat{h}(\xi) = \hat{f}(\xi - \xi_0)$.

Time scaling

For a non-zero real number a , if $h(x) = f(ax)$, then

$$\hat{h}(\xi) = \frac{1}{|a|} \hat{f}\left(\frac{\xi}{a}\right).$$

The case $a = -1$ leads to the *time-reversal* property, which states: if $h(x) = f(-x)$, then $\hat{h}(\xi) = \hat{f}(-\xi)$.

Conjugation

If $h(x) = \overline{f(x)}$, then

$$\hat{h}(\xi) = \overline{\hat{f}(-\xi)}.$$

In particular, if f is real, then one has the *reality condition*

$$\hat{f}(-\xi) = \overline{\hat{f}(\xi)},$$

that is, \hat{f} is a Hermitian function. And if f is purely imaginary, then

$$\hat{f}(-\xi) = -\overline{\hat{f}(\xi)}.$$

Integration

Substituting $\xi = 0$ in the definition, we obtain

$$\hat{f}(0) = \int_{-\infty}^{\infty} f(x) dx.$$

That is, the evaluation of the Fourier transform at the origin ($\xi = 0$) equals the integral of f over all its domain.

Discrete Fourier Transforms

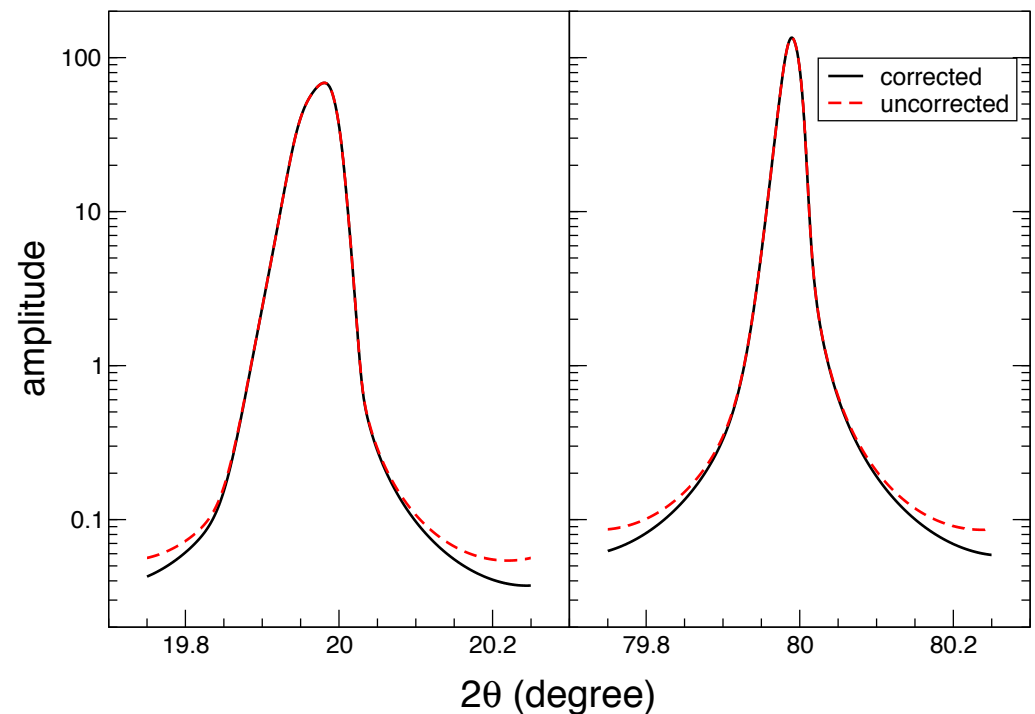
- Have a space of n bins separated by Δx . Will transform into discrete ω bins
- ω bin width, $\Delta\omega$, is $2\pi / (n \Delta x)$.
 - ω_{\min} is $-(n/2 - 1) \Delta\omega$,
 - ω_{\max} is $(n/2) \Delta\omega$
- DFT/FFT of a real function (intensity!) is entirely specified by the $+\omega$ part, since $-\omega$ is just complex conjugate.
- some real-function DFT/FFT packages put ω_{\max} in imaginary part of zero-frequency bin, and return $n/2$ imaginary numbers. Others (numpy, scipy, *e.g.*) return $n/2 + 1$ bins, with ω_{\max} in highest bin, where it naturally makes sense. This is very convenient.

Features of Fourier Space

- Efficient convolutions, as seen in previous slide
- Many of the broadenings we will look at have exact Fourier representations, so $\mathcal{F}(f(x))$ is generated directly, not by transforming $f(x)$.
 - Not (easily) true of axial divergence...
- The frequency scale of these transforms ($\lambda\omega/\cos\theta$) (with ω in inverse radians) actually has units of physically interpretable length! This will provide direct information about crystallite microstructure (see Bertaut, *Acta Cryst A*, **1950**, (3) 14)
- The same length scale information also can be used to directly understand the limits of the resolution of an instrument.

Periodic Boundary Conditions

- Fourier convolutions assume periodic functions
- If the tails are fall rapidly to zero, no problem.
- Numerous components have Lorentzian tails, which fall very slowly.
- Weird wrapping at tails, which is bad for peak computation
- Can be removed in real space if tails are Lorentzian.



from JRNIST, FPAPC

What is the FPA?

- In the FPA, the goal is to compute the line shape from first principles as a convolution of contributions from known sources.
 - need to know detailed instrument geometry
 - need to know detailed source X-ray spectrum
 - may have some well-known data on sample (density, composition)
- Remaining properties of line shape are probably interesting
 - corrected line position, to get lattice parameters
 - corrected line shape, to get microstructure
 - corrected line intensity, to get composition

Why isn't it trivial to calculate?

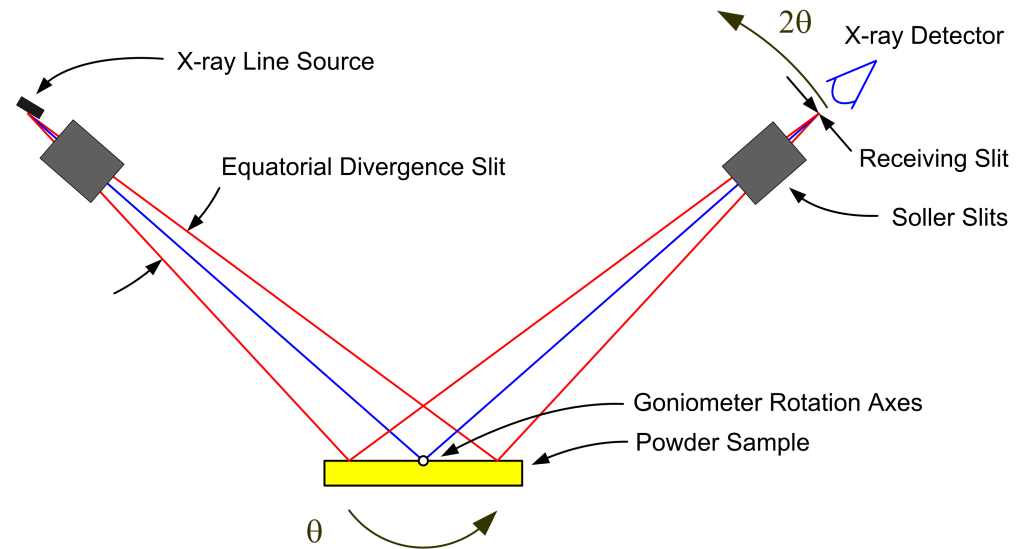
- need to get convolutions in way that preserves moments at very high accuracy (much less than the sampling interval)
- have Lorentzian tails, which converge very slowly and violate the requirement in the central limit theorem of finite second moments
- have $1/\sqrt{x}$ divergences
- have some components that need to be integrated in real space before converting to Fourier space

types of components of FPA

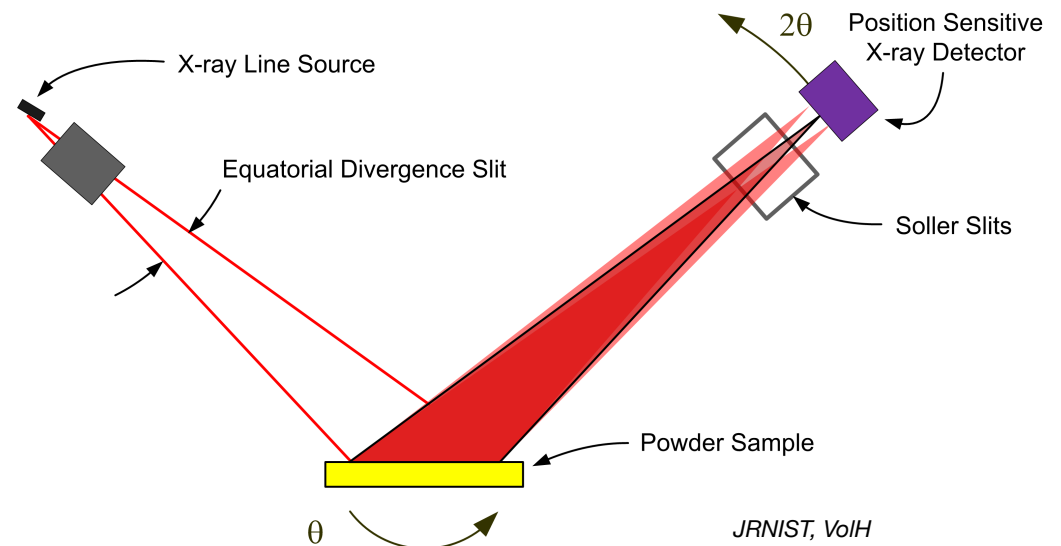
- Lorentzian broadening from intrinsic x-ray emission line shape, and from Lorentzian shape from size distribution and ad hoc Lorentzian microstrain
- Gaussian from ad hoc Gaussian size tails, from fitted estimates of spectrum as Gaussian, and ad hoc Gaussian microstrain
- $1/\sqrt{x}$ mostly from Debye cone, and from flat specimen
- rectangular, from slits
- other, messier bits from, e.g. sum of erf in Fourier space from log-normal particle size distributions

Fully Modeled Instruments

- Divergent Beam Bragg-Brentano with point detector (typically scintillator with slit)

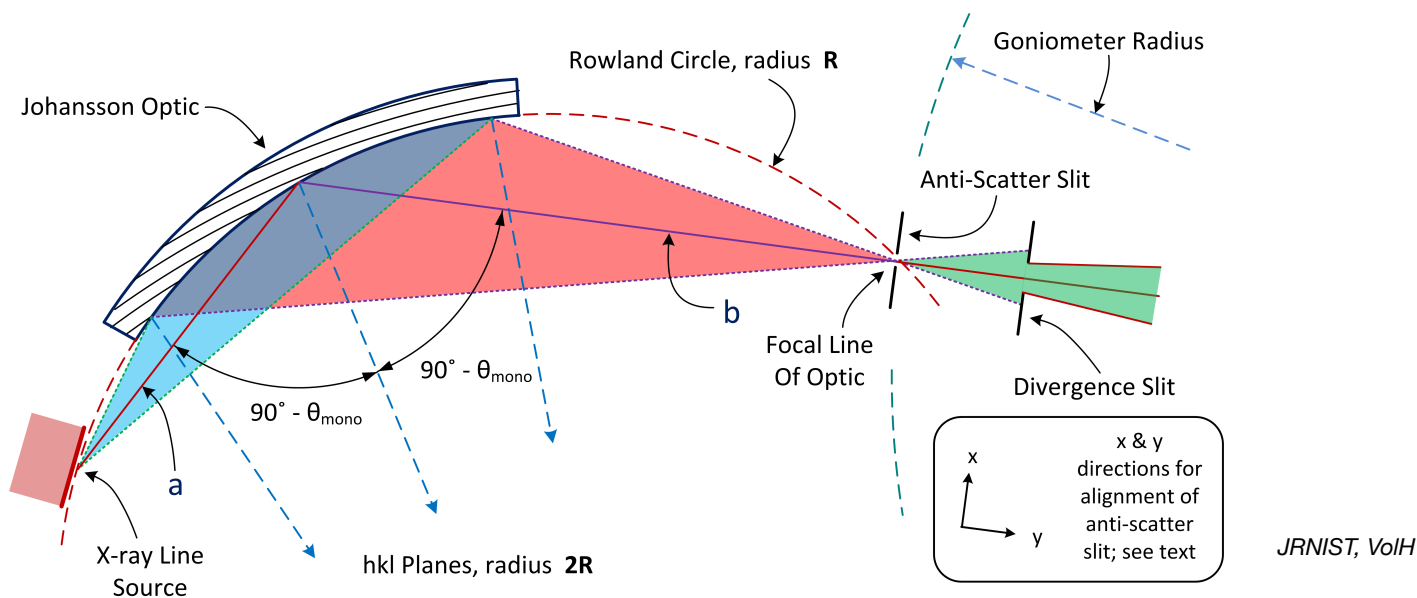


- Divergent Beam Bragg-Brentano with linear Position Sensitive Detector (PSD)



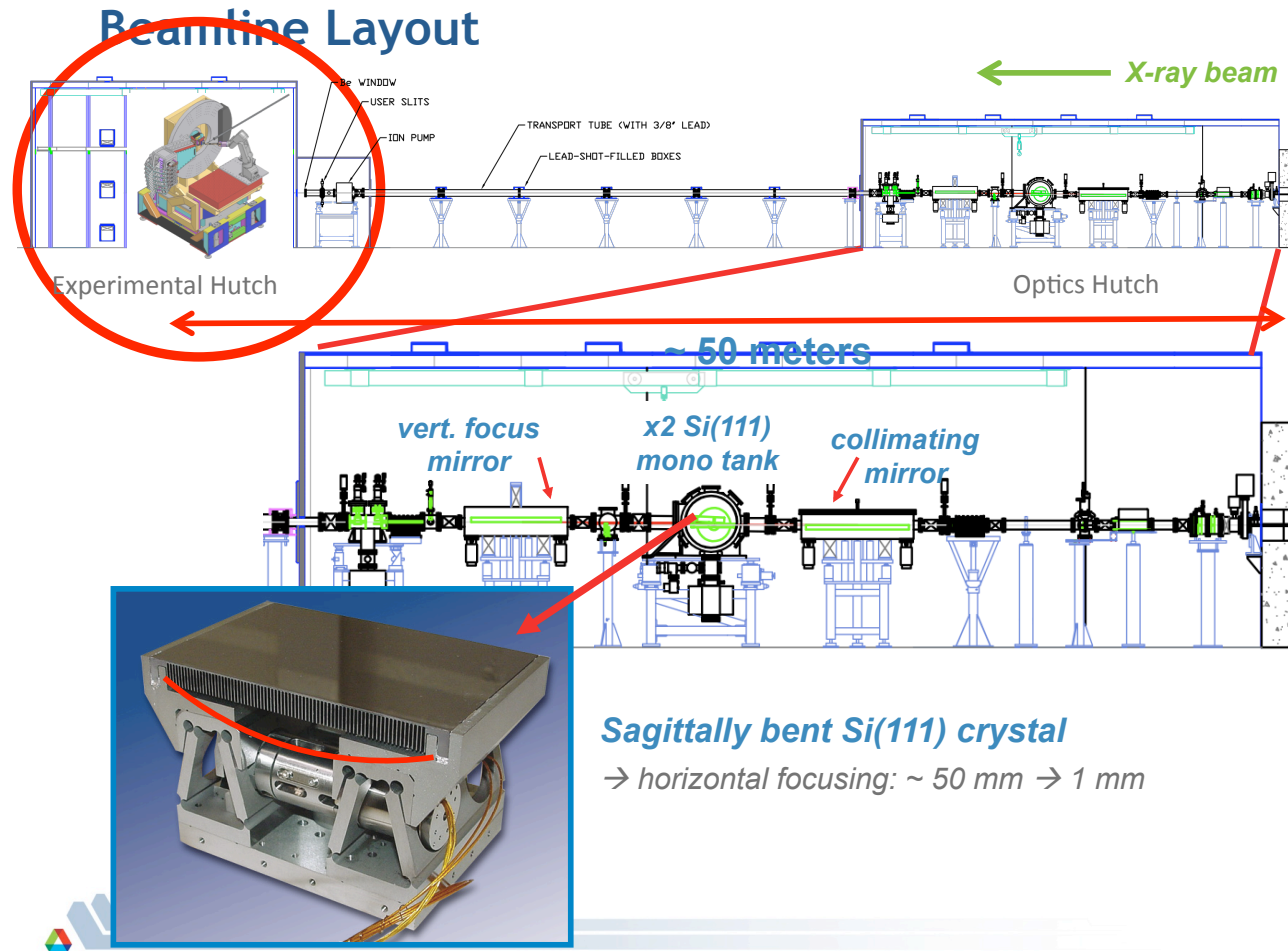
JRNIST, VolH

Well Modeled Instruments



- Divergent Beam Bragg-Brentano with Johansson optic and either point detector or PSD

Not-quite Modeled Instruments



5

- Typical Synchrotron powder diffraction beamline
http://11bm.xray.aps.anl.gov/documents/11BM_12SlideOverviewPresentation.pdf

Axial Divergence

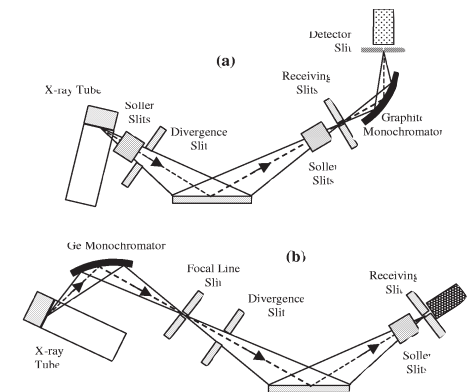
- Refers to beam angles perpendicular to the diffraction plane.
- Primary contribution to FPA, and trickiest to compute. Especially important due to asymmetry.
- Result of overlap of curved Debye cone and linear slits
- arc length (intensity) in slit is:

$$s = 2 r_D \left[\sin^{-1} \left(\sqrt{\frac{y_1}{2r_D}} \right) - \sin^{-1} \left(\sqrt{\frac{y_0}{2r_D}} \right) \right] \quad \text{'y' measured from apex}$$

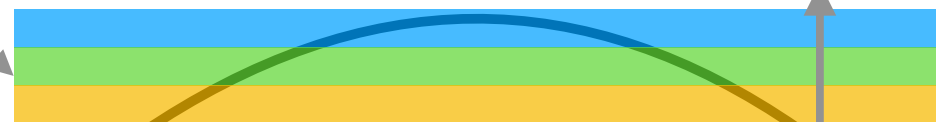
$$s \approx \sqrt{2 r_D} [\sqrt{y_1} - \sqrt{y_0}]$$

small angle approx, usually good

geometry reminder:
axial is out of plane



Slit scanned across peak

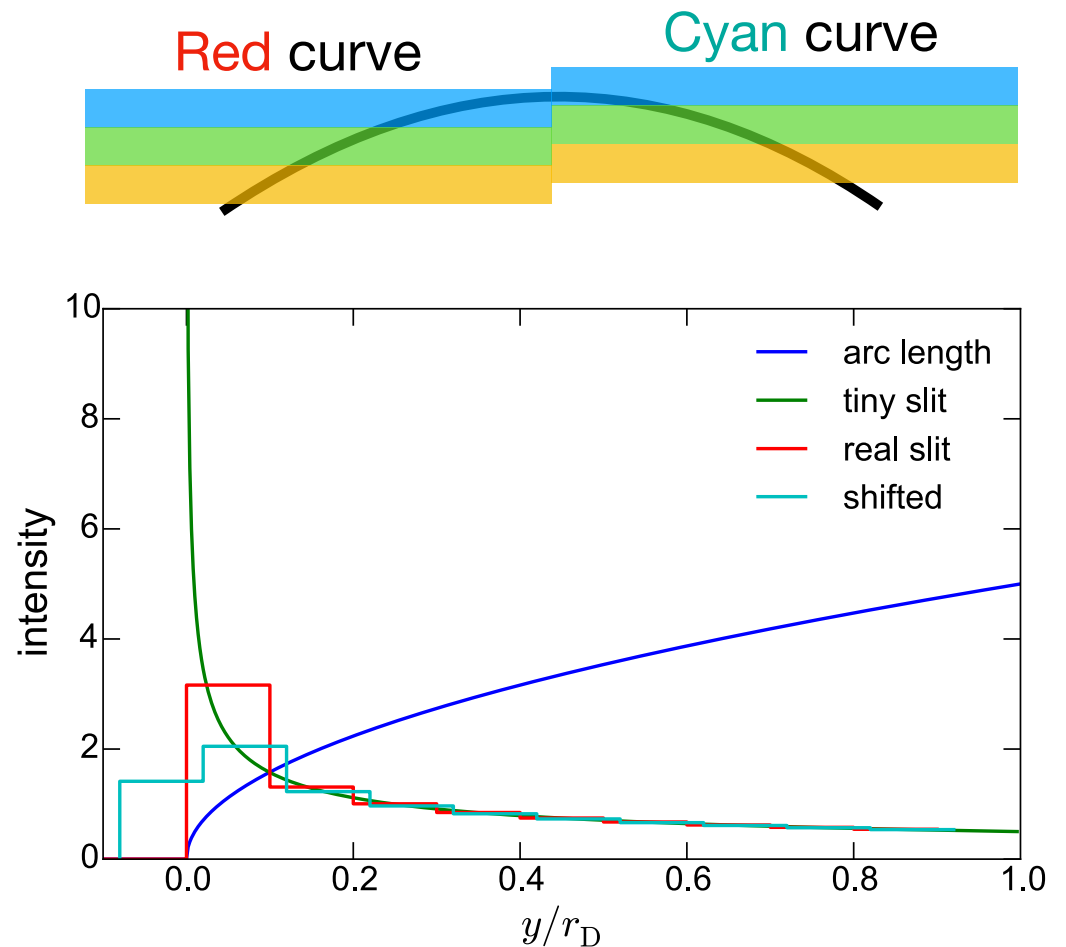


increasing θ_B

piece of Debye cone,
 $r_D = R \tan \theta_B$

Axial Divergence — 2

- **Blue** curve: 's' from previous slide
- **Green** curve: differential intensity, goes to infinity at edge of Debye cone. Numerically very bad $1/\sqrt{x}$
- **Red** curve: integrated intensity for detector with finite slit stepping across Debye cone. Numerically fine, if careful about partial bins.
- **Cyan** curve: steps not perfectly aligned to coincide with edge of Debye cone (real case...)
 - this binning handled very carefully in FPAPC 'axial_helper()' function.



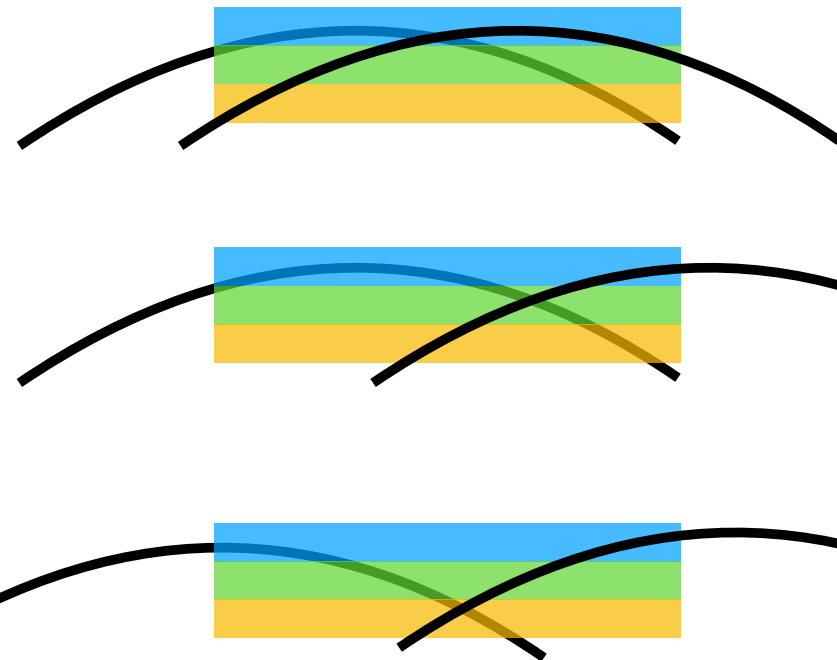
Axial Divergence — 3

- Finite source width in axial direction, finite width of sample, and finite receiver slits result in Debye cone being cut off in many ways.
- Table below shows complexity of this

condition 1		and			condition 2	
$r_\beta \downarrow \setminus \varepsilon \rightarrow$		ε_a	ε_b		ε_c	ε_d
$L_r > Z_0^+ - Z_0^-$		$Z_0^+ \leq \frac{L_r}{2}$ and $Z_0^- \geq -\frac{L_r}{2}$				
1		ε_1^+	ε_2^+		ε_1^-	ε_2^-
		$(Z_0^+ > \frac{L_r}{2} \text{ and } Z_0^- < \frac{L_r}{2}) \text{ or } (Z_0^+ > -\frac{L_r}{2} \text{ and } Z_0^- < -\frac{L_r}{2})$				
2		ε_2^+	ε_1^+		ε_1^-	ε_2^-
		any other range of Z_0				
3		ε_2^+	ε_1^+		ε_1^-	ε_2^-
$L_r < Z_0^+ - Z_0^-$		$Z_0^+ \geq \frac{L_r}{2}$ and $Z_0^- \leq -\frac{L_r}{2}$				
1		ε_1^-	ε_2^+		ε_1^+	ε_2^-
		$(Z_0^+ > \frac{L_r}{2} \text{ and } -\frac{L_r}{2} < Z_0^- < \frac{L_r}{2}) \text{ or } (-\frac{L_r}{2} < Z_0^+ < \frac{L_r}{2} \text{ and } Z_0^- < -\frac{L_r}{2})$				
2		ε_2^+	ε_1^-		ε_1^+	ε_2^-
		any other range of Z_0				
3		ε_2^+	ε_1^-		ε_1^+	ε_2^-

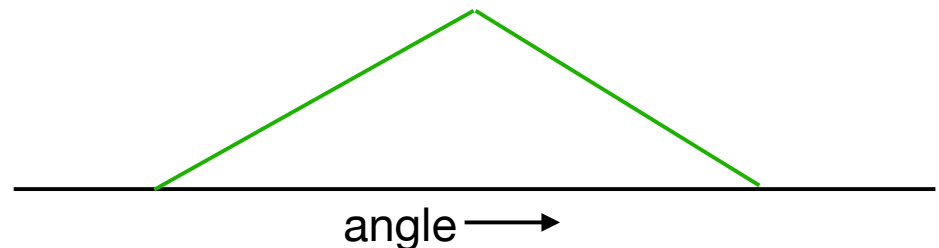
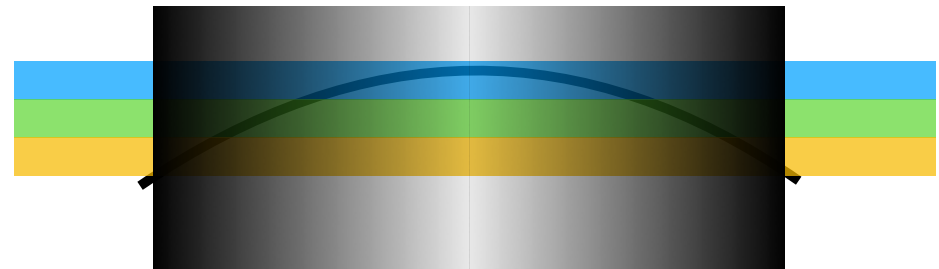
Table 1: Selection of computation boundaries and β ranges

JRNIST, FPAPC



Axial Divergence — Soller slits

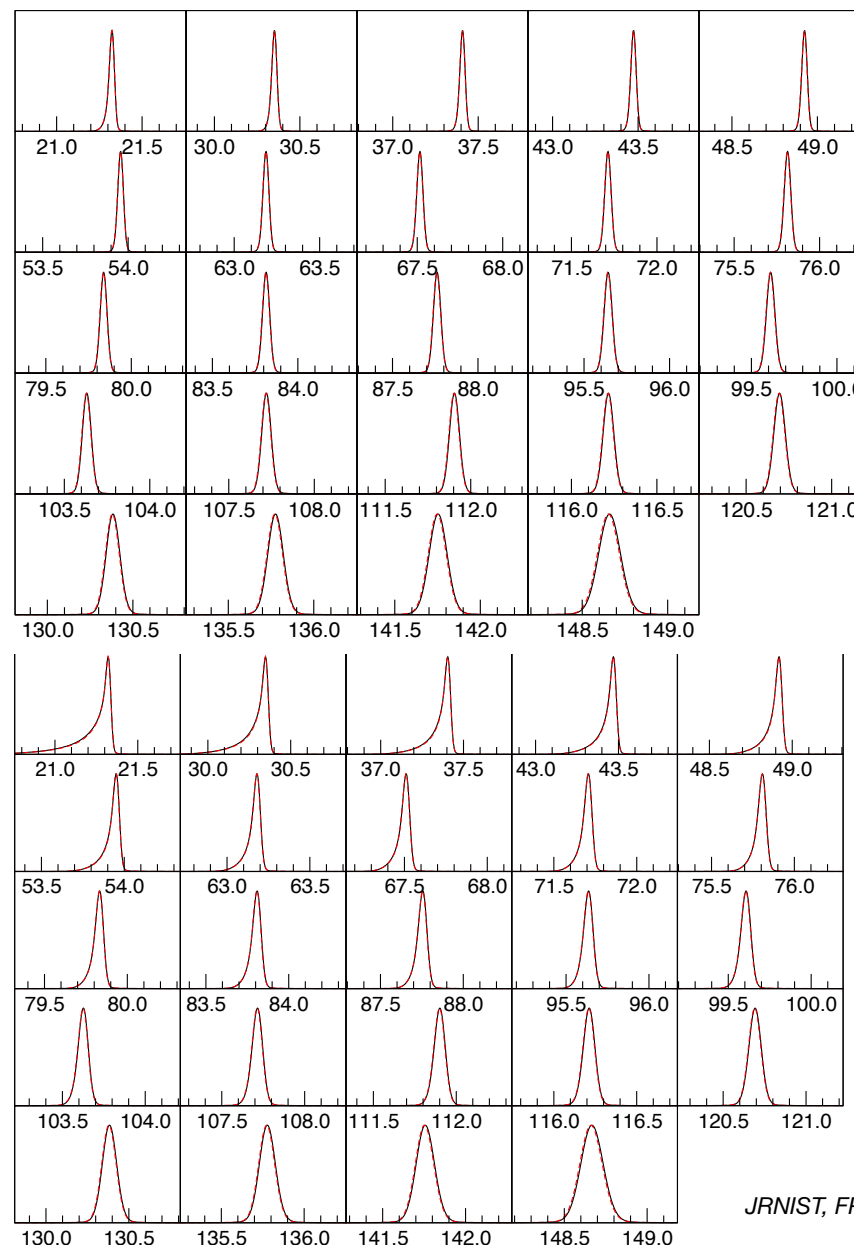
- Soller slit on detector trivially multiplies intensity from Debye cone by triangular transmission function. Reduces peak asymmetry (at cost of intensity).
- Soller slit on source is more complex, changes distribution of off-axis angles. Out-of-plane angle of beam from source is β in papers. Must integrate over correlated transmission of slit pair explicitly. This is the ' I_3 ' function of Cheary & Coelho
- Note that curvature (from 2 slides ago) depends on $y/\tan \theta_B$. This vanishes at 90° . No axial broadening in mid-angle region.



Soller slit transmission

Soller slit illustration

- Soller slits at 2.5 degrees. Note low-angle peaks, especially, remain fairly sharp.
- Soller slits at 10 degrees (*i.e.* wide open). The axial divergence function is extremely visible on the low-angle peaks.

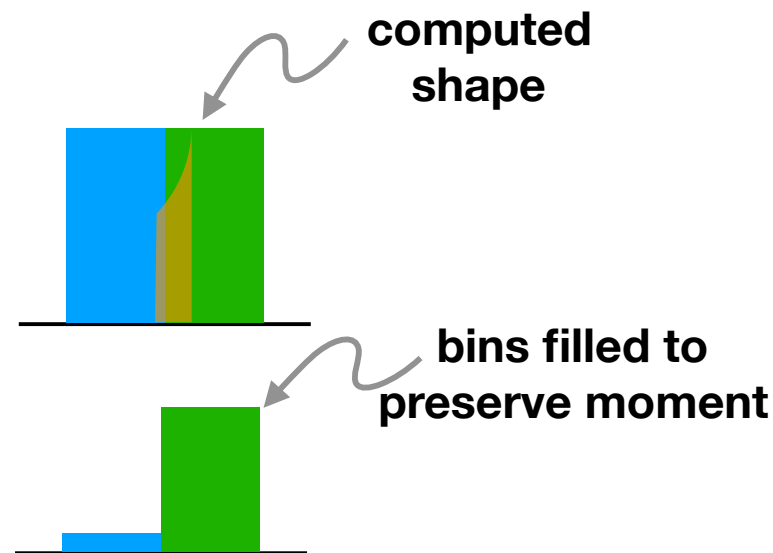


JRNIST, FPAPC

Axial Divergence — moments

- Precise peak position determination, for lattice measurement, requires conserving the first moment (centroid) of aberrations to sub-bin accuracy
- The general form of the axial divergence correction is at the top. The exact first moment is obtained by the usual weighted integral.
- Need to use this in degenerate cases in which the axial correction is less than 2 bins wide, to balance two bins to keep this correct.

$$y = y_0 + \frac{k}{\sqrt{x}}$$
$$\langle x \rangle = \frac{\int_{x_0}^{x_1} x y(x) dx}{\int_{x_0}^{x_1} y(x) dx}$$
$$\langle x \rangle = \frac{4k \left(x_1^{3/2} - x_0^{3/2} \right) + 3y_0 \left(x_1^2 - x_0^2 \right)}{12k \left(x_1^{1/2} - x_0^{1/2} \right) + 6y_0 \left(x_1 - x_0 \right)}$$



■ ■ ■

- The X-ray source energy or wavelength spectrum can be decomposed often into Voigt functions (Lorentzian-Gaussian convolutions).

$$V(\alpha, \sigma; x) = \int_{-\infty}^{+\infty} \frac{e^{-t^2/2\sigma^2}}{(x-t)^2 + \alpha^2} dt$$

- The Fourier transform of these is analytic.

$$\mathcal{F}[V(\alpha, \sigma; x - x_0)] = \exp \left[-\frac{\sigma^2 \omega^2}{2} - \alpha |\omega| - i\omega x_0 \right]$$

- A sum of these transforms, weighted by the line intensities, is the convolver for the spectrum.

- Note: if a monochromator is in use, there is no nice, exact expression. Typically approximate as a sum of Gaussians.

$$f(\omega) = \sum_{i=1}^n a_n \exp \left[-\frac{\sigma_n^2 \omega^2}{2} - \alpha_n |\omega| - i\omega x_n \right]$$

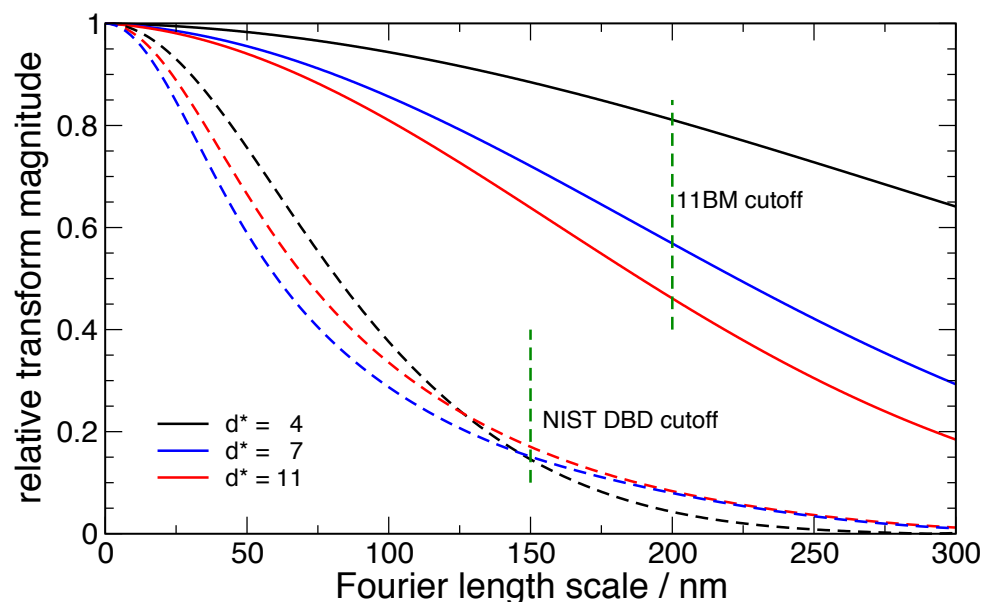
Flat specimen and linear PSD

- in Mathematica notebook
- These two aberrations are best written down from a single set of ray traces, since they depend on reflecting off of a flat sample
- equations then get integrated over sample surface and detector face
- the integral over a rectangular sample surface yields the classical flat-specimen correction that has the same $1/\sqrt{x}$ character as the axial divergence. It is handled in the FPAPC code by the same `axial_helper` function.
- The integral over an LPSD face yields a new aberration, which is described in FPAPC.

Understanding the IPF

- The Instrument Profile Function computed from the FPA can provide guidance about sources of uncertainty.
- Information about true peak shape requires, in one way or another, deconvolution of the IPF, which is division.
- In Fourier space, it is particularly easy to understand the impact. If the relative IPF is $\ll 1$, information is highly attenuated, and sensitive to noise and instrumental effects.
- This sets the limits on crystallite size determination

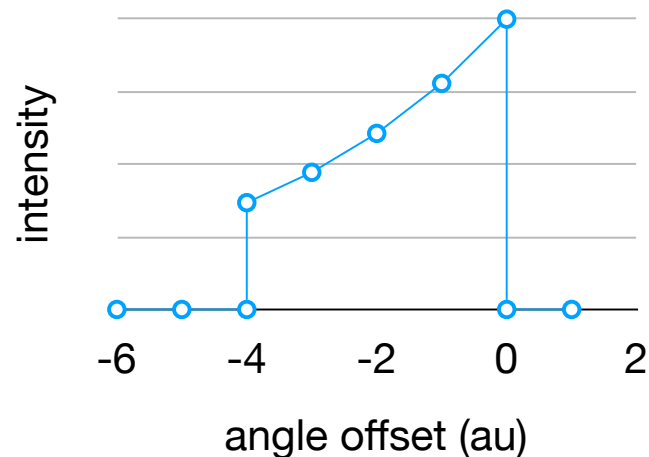
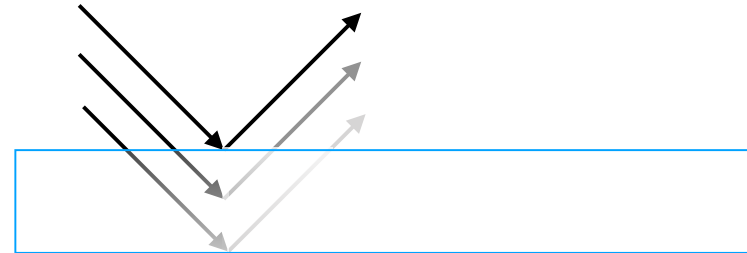
magnitude of the Fourier transform of FPA profiles computed for different instruments



length scale is $\lambda \omega / \cos\theta$,
 ω in radians⁻¹

Sample Transparency

- In Bragg-Brentano, with a weakly absorbing sample, the 'surface' is actually a region of exponential attenuation of the beam. This broadens and shifts peaks.
- Side note: $g(0) \neq 1$, not area conserving if $T < \infty$. x-rays lost out the back.



$$J_{\mu}(\epsilon) = \frac{\exp \frac{\epsilon}{\delta}}{\delta \left(1 - \exp \frac{\epsilon_{\min}}{\delta}\right)} \text{ where } \epsilon_{\min} < \epsilon < 0$$

$$\epsilon_{\min} = \frac{-2T \cos \theta_0}{R}$$

$$\delta = \frac{\sin 2\theta_0}{2\mu R}$$

$$g(\vec{\omega}) = \frac{1}{\delta} \frac{1 - \exp(\epsilon_{\min}(i\vec{\omega} + (1/\delta)))}{i\vec{\omega} + (1/\delta)}$$

Sample microstructure

- Defects in samples broaden peaks, with varying dependence on diffraction angle. Crystallite (domain) boundaries also broaden peaks. Beware of possible huge difference in physical particle size and crystallite size as seen by diffraction. See Bertaut, *Acta Cryst A*, **1950**, (3) 14 (in French)
- Simplest models contribute Lorentzian and Gaussian convolvers to the observed peak shape.
- Scardi & Leoni (*Acta Cryst.* (2001). **A57**, 604–613) worked out fairly detailed extension of Krill & Birringer (*Phil Mag. A* (1998). **v77 no. 3**, 621 —640) log-normal crystallite size distribution peak shape for some crystallite shapes. Result is sum of error functions in Fourier space.
- Code for this is available as a plugin to FPAPC on request. It includes hexagonal prisms, not part of S&L. Hex also available as a Topas 4 or 5 include file.

Comments on use of the FPA

- If we have correctly computed the intrinsic peak shape, we can synthesize peaks in 2θ or Fourier space
- This only works if we have a really accurate FPA IPF. It should be based on as many directly (or, at least, independently of the current experiment) measured parameters of the diffractometer as possible.
- Use of a sample with very sharp peaks, such as SRM 660c (very high attenuation, ideal), or SRM 640d (lower attenuation, still sharp peaks) allows one to verify the FPA results without the real peak width being tangled up in the IPF.

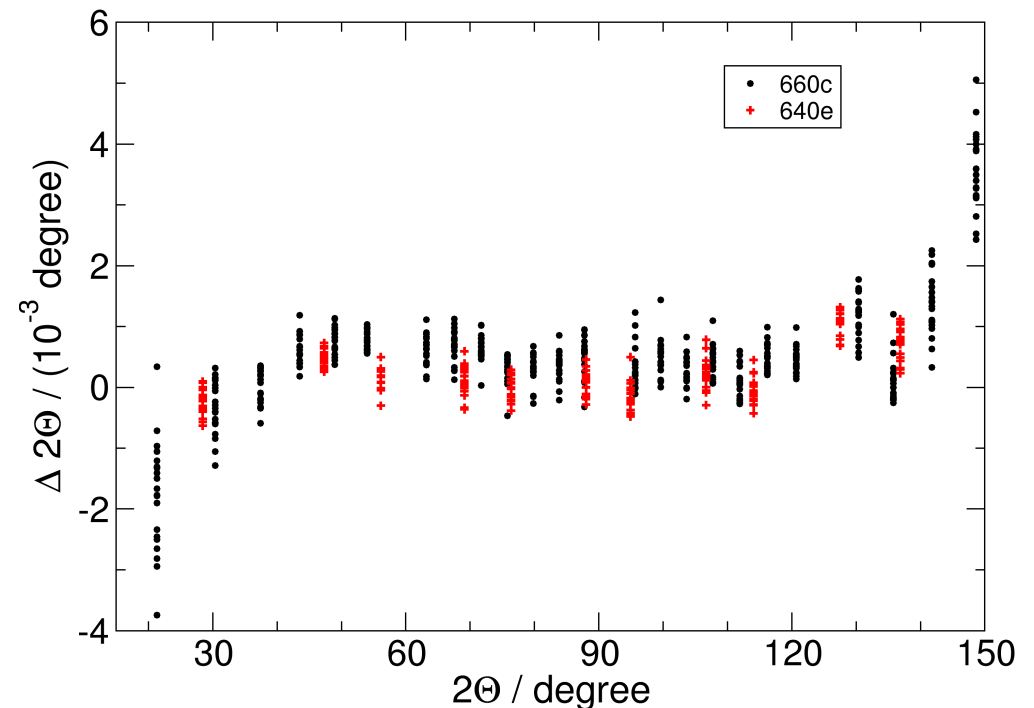
Using the FPA in 2θ space

- The FPA can be used to synthesize peak shapes, including the IPF and sample characteristics. These can be fed into a least-squares fitter either for
 - Pawley fits (position fixed by symmetry group & lattice, intensity is free parameter), or,
 - Rietveld fits (intensities computed from structure)
- FPAPC has a simple interface for peak synthesis. It does not incorporate the least-squares fitting or structure models.
- Fitting is what packages like TOPAS* do. Work is underway for this in GSAS-II. Also, xrayutilities (a pure-python package) has incorporated the NIST FPAPC.

*Certain commercial equipment, instruments, or materials are identified in this paper in order to specify the experimental procedure adequately. Such identification is not intended to imply recommendation or endorsement by the U.S. government, nor is it intended to imply that the materials or equipment identified are necessarily the best available for the purpose.

Peak position accuracy in FPA

- Use of a full FPA-based Pawley fit can result in very high accuracy peak positions
- Data at right from open-beam (no IBM) scans of SRM 660c (LaB₆) and SRM 640e (Si)
- These positions do not depend on interpolating peaks from a known standard material and using a parameterized asymmetry model.

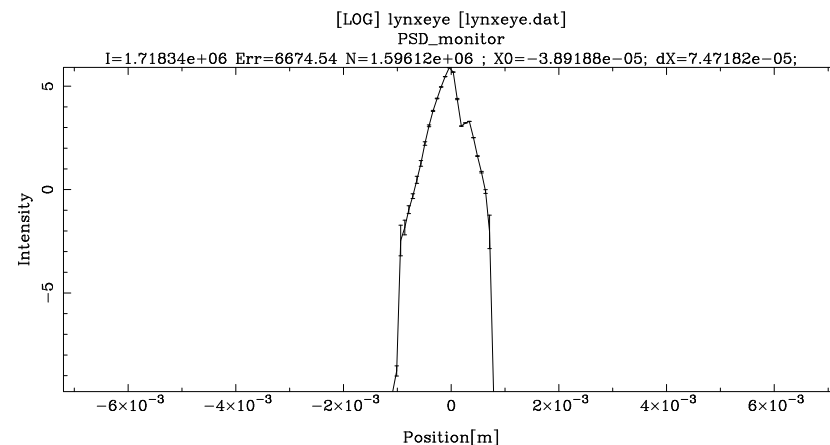
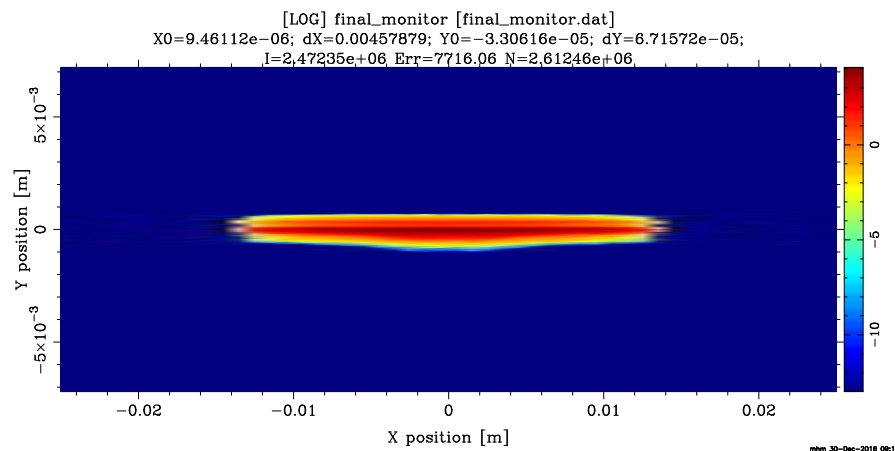


Using the FPA in Fourier space

- In Fourier space, by dividing out the transform of the IPF from the observed transform, what is left is exactly the function described in Bertaut. The second derivative of this function is the differential column length distribution.
- FPAPC can directly return the Fourier transform of the peak for this type of analysis. This was used in the certification of SRM 1979, an SRM with microstructure-broadened peaks.
- see https://www-s.nist.gov/srmors/view_detail.cfm?srm=1979

Comparison to Monte Carlo

- The gold standard for working out the behavior of a complex optical system is Monte Carlo ray tracing
- Can be 'exact' with limits of underlying diffraction theory
- Packages such as McXTrace allow one to set up fully detailed models, with all slits, collimators, optics, etc.
- here: simulation of DBD and IBM, as a function of focus error of IBM
- will use to test validity limits of FPA



Some FPAPC details

- FPAPC class represent a single peak with all instrument and material parameters
- FPAPC caches convolves that are unchanged, to allow efficient use with minimal recompilation in fitting or optimization procedures
- an add-on class makes a list-like object of peak classes which can be evaluated in parallel on multiprocessing architectures to improve speed
- FPAPC is extensible; it automatically looks for specially named functions to find new convolves which have been added via mixing classes
- FPAPC includes doxygen comments to allow generation of a user manual

equation of sample passing through origin at angle ω

$$\mathbf{x1} = \{t \cos[\omega], t \sin[\omega]\}$$
$$\{t \cos[\omega], t \sin[\omega]\}$$

equation of beam at angle α from centerline, starting at $[-R, 0]$

$$\mathbf{r1} = \{s \cos[\alpha] - R, s \sin[\alpha]\}$$
$$\{-R + s \cos[\alpha], s \sin[\alpha]\}$$

point where beam strikes sample

$$\mathbf{p1} = \mathbf{x1} /. \text{Solve}[\mathbf{x1} == \mathbf{r1}, \{t\}, \{s\}][[1]]$$
$$\{-((R \cos[\omega] \sin[\alpha]) / (\cos[\omega] \sin[\alpha] - \cos[\alpha] \sin[\omega])), -(R \sin[\alpha] \sin[\omega]) / (\cos[\omega] \sin[\alpha] - \cos[\alpha] \sin[\omega])\}$$

outgoing ray starting from p_1 at angle $2\phi + \alpha$ where 2ϕ is $2\theta_B$

$$\mathbf{r2} = \mathbf{p1} + s \{\cos[2\phi + \alpha], \sin[2\phi + \alpha]\}$$
$$\{s \cos[\alpha + 2\phi] - (R \cos[\omega] \sin[\alpha]) / (\cos[\omega] \sin[\alpha] - \cos[\alpha] \sin[\omega]), s \sin[\alpha + 2\phi] - (R \sin[\alpha] \sin[\omega]) / (\cos[\omega] \sin[\alpha] - \cos[\alpha] \sin[\omega])\}$$

detector plane is line through $R \{\cos[\theta_2], \sin[\theta_2]\}$, perpendicular so that

$$\text{detline} = t \{-\sin[\theta_2], \cos[\theta_2]\} + R \{\cos[\theta_2], \sin[\theta_2]\}$$
$$\{R \cos[\theta_2] - t \sin[\theta_2], t \cos[\theta_2] + R \sin[\theta_2]\}$$

these lines intersect and the parameter t is the position on the detector face

$$\text{dethit} = t /. \text{Solve}[\mathbf{r2} == \text{detline}, \{t\}, \{s\}][[1]]$$
$$-((-\sin[\alpha + 2\phi] (-R \cos[\theta_2] - (R \cos[\omega] \sin[\alpha]) / (\cos[\omega] \sin[\alpha] - \cos[\alpha] \sin[\omega])) + \cos[\alpha + 2\phi] (-R \sin[\theta_2] - (R \sin[\alpha] \sin[\omega]) / (\cos[\omega] \sin[\alpha] - \cos[\alpha] \sin[\omega])))) / (-\cos[\theta_2] \cos[\alpha + 2\phi] - \sin[\theta_2] \sin[\alpha + 2\phi]))$$

hitoffset is the distance from the center of the detector at which the ray strikes, and ϵ is the offset from the actual double diffraction angle and the detector position

$$\begin{aligned} \text{hitoffset} &= \text{Simplify}[\text{TrigExpand}[\text{dethit} /. \theta 2 \rightarrow 2\phi + \epsilon]] \\ &= \frac{1}{2} R \text{Csc}[\alpha - \omega] \text{Sec}[\alpha - \epsilon] (\text{Cos}[2\alpha - \epsilon - \omega] - \text{Cos}[\epsilon - \omega] - 2 \text{Sin}[\alpha] \text{Sin}[\alpha + 2\phi - \omega]) \end{aligned}$$

expand hit offset in α, ϵ

$$\begin{aligned} \text{ser} &= \text{Series}[\text{hitoffset}, \{\alpha, 0, 2\}, \{\epsilon, 0, 2\}] \\ &= (-R\epsilon + O[\epsilon]^3) + \left((R - R \text{Csc}[\omega] \text{Sin}[2\phi - \omega]) + \left(R - \frac{1}{2} R \text{Csc}[\omega] \text{Sin}[2\phi - \omega] \right) \epsilon^2 + O[\epsilon]^3 \right) \alpha + \\ &\quad \left((-R \text{Cos}[2\phi - \omega] \text{Csc}[\omega] - R \text{Cot}[\omega] \text{Csc}[\omega] \text{Sin}[2\phi - \omega]) + (-R + R \text{Csc}[\omega] \text{Sin}[2\phi - \omega]) \epsilon + \right. \\ &\quad \left. \left(-\frac{1}{2} R \text{Cos}[2\phi - \omega] \text{Csc}[\omega] - \frac{1}{2} R \text{Cot}[\omega] \text{Csc}[\omega] \text{Sin}[2\phi - \omega] \right) \epsilon^2 + O[\epsilon]^3 \right) \alpha^2 + O[\alpha]^3 \end{aligned}$$

the $R\epsilon$ term is what the PSD software corrects for by sliding the spectrum, so the second term is the aberration. Expressed as an angle by dividing by R

$$\begin{aligned} &\text{Collect}[\text{Normal}[\text{Simplify}[\text{ser} / R + \epsilon]], \alpha] \\ &= \alpha^2 (-\epsilon^2 \text{Cos}[\phi] \text{Csc}[\omega]^2 \text{Sin}[\phi] - \text{Csc}[\omega]^2 \text{Sin}[2\phi] + 2\epsilon \text{Cos}[\phi] \text{Csc}[\omega] \text{Sin}[\phi - \omega]) + \\ &\quad \alpha \left(-2 \text{Cos}[\phi] \text{Csc}[\omega] \text{Sin}[\phi - \omega] + \epsilon^2 \left(1 - \frac{1}{2} \text{Csc}[\omega] \text{Sin}[2\phi - \omega] \right) \right) \end{aligned}$$

The α, ϵ^0 term is the classical defocusing if ϕ is close to ω , i.e. $-2 \alpha \text{Sin}[\phi - \omega] / \text{Tan}[\phi]$

The α^2, ϵ^0 term is the classical ‘flat specimen’ correction, since $\text{Csc}[\omega]^2 \text{Sin}[2\phi]$ reduces to $1 / \text{Tan}[\phi]$ if $\omega = \phi$

The α^2, ϵ^2 term, if $\phi = \omega$, is $\alpha \epsilon^2 / 2$ and, essentially, $\epsilon = \phi - \omega$ so the aberration is $\alpha (-2 \epsilon / \text{Tan}[\phi] + \epsilon^2 / 2)$

Note that for a detector which is 0.03 radians wide (7 mm at 217 mm), the 2ϵ term hugely dominates the ϵ^2 term